Modified beam theories for bending properties of nanowires considering surface/intrinsic effects and axial extension effect

H. F. Zhan and Y. T. Gu

Citation: J. Appl. Phys. **111**, 084305 (2012); doi: 10.1063/1.3703673
View online: http://dx.doi.org/10.1063/1.3703673
View Table of Contents: http://jap.aip.org/resource/1/JAPIAU/v111/i8
Published by the American Institute of Physics.

Modified beam theories for bending properties of nanowires considering surface/intrinsic effects and axial extension effect

H. F. Zhan and Y. T. Gu[a)]
School of Chemistry, Physics and Mechanical Engineering, Queensland University of Technology, Brisbane 4001, Australia

(Received 27 January 2012; accepted 10 March 2012; published online 18 April 2012)

Several studies of the surface effect on bending properties of a nanowire (NW) have been conducted. However, these analyses are mainly based on theoretical predictions, and there is seldom integration study in combination between theoretical predictions and simulation results. Thus, based on the molecular dynamics (MD) simulation and different modified beam theories, a comprehensive theoretical and numerical study for bending properties of nanowires considering surface/intrinsic stress effects and axial extension effect is conducted in this work. The discussion begins from the Euler-Bernoulli beam theory and Timoshenko beam theory augmented with surface effect. It is found that when the NW possesses a relatively small cross-sectional size, these two theories cannot accurately interpret the true surface effect. The incorporation of axial extension effect into Euler-Bernoulli beam theory provides a nonlinear solution that agrees with the nonlinear-elastic experimental and MD results. However, it is still found inaccurate when the NW cross-sectional size is relatively small. Such inaccuracy is also observed for the Euler-Bernoulli beam theory augmented with both contributions from surface effect and axial extension effect. A comprehensive model for completely considering influences from surface stress, intrinsic stress, and axial extension is then proposed, which leads to good agreement with MD simulation results. It is thus concluded that, for NWs with a relatively small cross-sectional size, a simple consideration of surface stress effect is inappropriate, and a comprehensive consideration of the intrinsic stress effect is required. © *2012 American Institute of Physics*. [http://dx.doi.org/10.1063/1.3703673]

I. INTRODUCTION

Nanowires (NWs) are receiving increasing applications in diverse areas, such as the nanocomposites strengtheners,[1] the active components of nanoelectromechanical systems including high frequency resonator,[2,3] force and pressure sensing,[4] ultrahigh-resolution mass sensing,[5] and other devices.[6,7] These nanowire-based devices are envisioned to quickly find their way into high-performance electronics and commercial products.[8] Therefore, it is of great importance from both scientific and technological viewpoints to investigate the mechanical properties of NWs. In the past decade, various experimental studies of NWs have been carried out. For instance, a number of atomic force microscope (AFM)-based compression, bending, and nanoindentation studies of NWs have been conducted.[9–12] Through *in situ* tensile experiments, Yue *et al.*[13] found Cu NWs could sustain ultrahigh elastic strains. The defect-free Au NWs are reported showing superplasticity on tensile deformation.[14] The size effects on elasticity, yielding, and fracture of five-fold twinned Ag NWs have been studied via *in situ* tensile experiments.[15] Meanwhile, the numerical approaches are also being frequently applied to investigate the NW's properties, such as *ab initio* calculation, multi-scale simulation, and molecular dynamic (MD) simulation. For example, the investigation of NWs mechanical properties under tensile deformation, including influences from factors of strain rate, temperature, surface defects, and others.[16–19] Other NW deformation situations such as compression and torsion are also being investigated.[20–22] A number of atomistic studies of NW bending behaviors have been reported, e.g., Zheng *et al*. reported the formation of two conjoint fivefold deformation twins in Cu NWs under bending.[23] McDowell *et al*. estimated the Young's modulus of Ag NWs during bending.[24] Wu investigated the bending response of a Cu cantilever NW by applying a lateral force at one end of the NW.[25]

It is generally accepted that the surface stress and surface elasticity play an important role in the mechanical properties of NWs. Researchers have reported a plethora of novel mechanical behaviors of NWs that arisen from the surface effect, such as the phase transformations phenomenon,[26] pseudoelastic behavior,[27] and shape memory effect.[28,29] By assuming that the overall elastic behavior of NW is a superposition of surface areas and bulk volume where the bulk volume exhibits the identical elastic properties as the corresponding macroscopic bulk material, researchers have proposed several theoretical analyses to characterize the surface effect under different deformation situations. For example, according to the classical Euler-Bernoulli beam theory and Timoshenko beam theory, Wang and Feng carried out a serial analysis of the surface stresses influence on the vibration and buckling behaviors of NWs.[30–33] A general discussion of the surface effect during the bending deformation are also well documented by previous researchers, e.g., the modified Euler-Bernoulli beam theory by He and Lilley,[34,35] and the modified

[a)]Author to whom correspondence should be addressed. Electronic mail: yuantong.gu@qut.edu.au. Telephone: +61-7-31381009. Fax: +61-7-31381469.

Timoshenko beam theory by Jiang and Yan.[36] A complete review of the surface stress effect in mechanics of nanostructure elements, including nanoparticles, NWs, moonbeams, and nanofilms can be found in the recent work by Wang *et al.*[37] Besides the theoretical study of the surface stress effects, the multi-scale simulations have also been conducted to investigate the bending behaviors and properties of Au NWs, which are achieved by utilizing the surface Cauchy-Born model.[38,39]

Although several discussions of the surface effect have been carried out, we note that these discussions are mainly based on the comparisons among different theoretical predictions, and rare open discussions between these different theoretical approaches and the MD simulation results are found. For instance, the work reported by He and Lilley is mainly based on Young's modulus obtained from the classical Euler-Bernoulli beam theory and modified Euler-Bernoulli beam theory.[34] Therefore, it is of great interest to investigate the applicability of different theoretical approaches during bending deformation. It is worthy to point out that, for the resonant frequencies, a comprehensive discussions between the theoretical predictions and MD results have already been reported by Olsson *et al.*[40] They found that Timoshenko beam theory performs better for small aspect ratio Au NWs due to shear and rotary inertial effects.

According to the AFM-bending approach proposed by Wu *et al.*,[41,42] a complete investigation of a three-point bending model by MD simulation for double clamped Cu NWs is conducted by our recent work.[43] It is found that such bending model could provide full spectrum of NW mechanical properties, ranging from elasticity, plasticity, and failure. Thus, based on this bending model and different modified beam theories, we provide a comprehensive theoretical and numerical study for bending properties of double clamped Ag NWs considering surface/intrinsic stress effects and axial extension effect. The discussion will begin from the Euler-Bernoulli beam theory and Timoshenko beam theory augmented with surface effect that proposed previously. Further investigations of the factors, including intrinsic stress and axial extension, that lead to the divergence between theoretical predictions and MD simulation results are then carried out.

II. NUMERICAL IMPLEMENTATION

MD three-point bending simulations are carried out on double clamped Ag NWs, which are performed by the large-scale Atomic/Molecular Massively Parallel Simulator.[44] Square cross-section Ag NW with the initial atomic configuration positioned at perfect FCC lattice site is considered, and the x, y, and z coordinate axes represent the lattice directions of [100], [010], and [001], respectively. As shown in Fig. 1(a), the NW is divided into two regions, including boundary region and mobile region. To mimic the clamped boundary condition, boundary regions in two ends are fixed in all three dimensions (x, y, and z). No periodic boundary condition is adopted. A rigid diamond cylinder tip is employed to impose the bending load. For convenience, the size of the NW is denoted as $h \times h \times L$, where h denotes the cross-section size and L denotes the length. Three groups of Ag NWs have been considered, as listed in Table I. According to the discussion

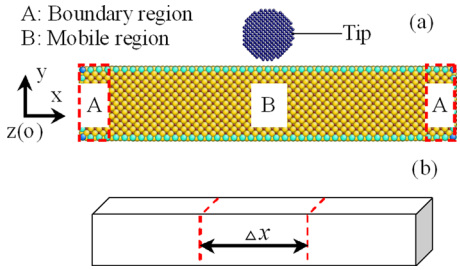

FIG. 1. (a) MD three-point bending simulation model of Ag NW. The NW is divided into two regions, including boundary region A and mobile region B. The rigid diamond cylinder tip is located right at the middle of NW; (b) axial virial stress calculation schematic. The virial stress is averaged over each column of atoms along the longitudinal direction (around the center region) with the distance of Δx.

by Liu and Rajapakse,[45] NWs in Group 1 with the slenderness ratio L/h between $12.5 \sim 50$ are taken as thin NWs, as well as NWs in Group 3 with a constant slenderness ratio of 15. NWs in Group 2 with the slenderness ratio ranging from $2.5 \sim 10$ are taken as thick NWs.

The embedded-atom-method potential developed by Voter[46] is used to describe the Ag-Ag atomic interactions in these simulations, which was fitted to a group of parameters, including cohesive energy, equilibrium lattice constant, bulk modulus, and others.[29] For the Ag-C atomic interaction, a Morse potential is applied.[47] The Ag lattice constant a is chosen as 0.409 nm.[46] The equations of motion are integrated with time using a velocity Verlet algorithm.[48] During each simulation, NWs are first relaxed to a minimum energy state using the conjugate gradient energy minimization and then the Nose-Hoover thermostat[49,50] is employed to equilibrate the NWs at 0.01 K. After that, a constant velocity is imposed to the rigid tip. More details of this simulation model could be found in our recent work.[43]

III. RESULTS AND DISCUSSIONS

Following the convention of the work by He and Lilley,[34] Young's modulus extracted from the classical Euler-Bernoulli beam theory (EBT-Classical), the classical Timoshenko beam theory (TBT-Classical), and experimental measurements is taken as overall Young's modulus E_{ov} and Young's modulus determined by other modified beam theories is taken as bulk Young's modulus E_b. In this work, Ag NW's experimental Young's modulus is chosen as 76 GPa,[51] which has been frequently cited. To note that, during the comparison of theoretical predictions and MD simulation results, the same fitting procedure adopted by previous

TABLE I. Simulation models summary. Three groups of NWs have been considered, including Group 1 with ten cases, and the NW length as 122.7 nm; Group 2 with ten cases, and the NW length as 24.54 nm; and Group 3 with eight cases, and the NWs have a uniform slenderness ratio L/h as 15. The Ag lattice constant a is chosen as 0.409 nm.

Group	Cross-sectional size h (nm)									
1	$6a$	$8a$	$10a$	$12a$	$14a$	$16a$	$18a$	$20a$	$22a$	$24a$
2	$6a$	$8a$	$10a$	$12a$	$14a$	$16a$	$18a$	$20a$	$22a$	$24a$
3	$6a$	$8a$	$10a$	$12a$	$14a$	$16a$	$18a$	$20a$		

researchers are employed,[43,52] i.e., using the data at small displacement to fit, and extend to include increasingly larger displacement. This procedure is employed as it could not only estimate the value of Young's modulus, but also reveal the accuracy of the theoretical prediction.

A. Thin nanowires

For the classical Euler-Bernoulli beam theory, the governing equation of the double clamped thin beam under pure bending is given as[53] (referred as EBT-Classical)

$$(EI)w^{iv} = 0, \tag{1}$$

where E is bulk Young's modulus, w is the beam deflection, I is the moment of inertia. For the square cross-section NW considered here, I equals $h^4/12$. The following notations are applied as $w' = dw/dx$, $w'' = d^2w/dx^2$, $w''' = d^3w/dx^3$, and $w^{iv} = d^4w/dx^4$.

As aforementioned, the surface stress has a significant influence on the mechanical properties of NWs. Wang and Feng[32] suggested that the surface effect can be expressed by surface elasticity and residual surface stress. According to the composite beam theory,[54] surface elasticity can be rationalized by replacing the classical flexural rigidity EI with the effective flexural rigidity $(EI)^*$. For the square cross-section beam, $(EI)^*$ is given as $(EI)^* = Eh^4/12 + 2E_sh/3$, where E_s is the surface elastic modulus.[33,34] For the NW under bending, a distributed transverse force caused by the surface residual stress is described by the generalized Young-Laplace equation.[33,55] This force is along the NW longitudinal direction, and expressed by $p(x) = Hw''$, where H is a constant parameter determined by the surface stress along the NW longitudinal direction and the NW cross-sectional shape. By neglecting the longitudinal extension of NWs, and assuming small deflection and deformation, He and Lilley[34] proposed the Euler-Bernoulli beam theory augmented with surface effect as (referred as EBT-Surface)

$$(EI)^*w^{iv} - Hw'' = 0. \tag{2}$$

Considering the small deformation approximation, H is simplified as $H = H^0 = 2\tau_0 h$, where τ_0 is the residual surface stress along NW longitudinal direction.

Equations (1) and (2) are solved subject to the usual clamped boundary conditions at both ends, with a constant load F applied at the midpoint $x = L/2$ of the NW, i.e., the transverse displacement and slope are zeros at $x = 0$, and the slope at $x = L/2$ is also zero because of symmetry. The force equilibriums at $x = 0$ are $-(EI)w''' = F/2$ and $-(EI)w''' = F/2 + \int_0^{L/2} H^0 w''dx = F/2$ for Eqs. (1) and (2), respectively. The relationship between the applied load F and the resulting displacement d can be deduced as given by Eqs. (3a) and (3b), respectively,

$$F = \frac{192EI}{L^3}d, \tag{3a}$$

$$F = 2H^0\left[\frac{L}{2} - \frac{L}{\sqrt{k_s}}\tanh(\sqrt{k_s}/4)\right]^{-1}d, \tag{3b}$$

where k_s is a nondimensional surface effect factor, and expressed as $k_s = H^0L^2/(EI)^*$. Based on these two equations, He and Lilley[34] calculated the overall Young's modulus of Ag NWs and Pb NWs and compared with experimental results. Some encouraging findings have been obtained, e.g., generally, the overall Young's modulus of Ag NWs is increasing along with decrease of diameter when the NW length is constant for both the EBT-Surface and experimental results from Jing *et al.*[51] As we note that comparisons made by He and Lilley[34] are mainly based on the Young's modulus obtained from Eqs. (3a) and (3b), which have predetermined the surface effect. In other words, the surface effect on NW bending properties is actually discussed among theoretical predictions, and no studies of the F-d curves that provided by the modified beam theories and simulation results have been conducted.

To investigate into our concerns about the surface effect, we begin the discussions from the comparisons between the theoretical predictions by Eqs. (3a) and (3b) and MD simulation results. These two equations are employed to fit with the MD simulation results from Group 1, with NWs possessing the same length but different cross-sectional sizes ranging from 2.454 nm to 9.816 nm (see Table I). The classical flexural rigidity EI in Eq. (3a) is replaced by the effective flexural rigidity $(EI)^*$ in the following context. The residual surface stress and the surface elasticity values for (100) Ag from atomistic calculations by Sheony[56] are adopted, i.e., $\tau_0 = 0.89\,\mathrm{N/m}$, $E_s = 1.22\,\mathrm{N/m}$. Since both Eqs. (3a) and (3b) have predicted a linear relationship between F and d, only MD simulation results that fall in the displacement between 0 and $0.5h$ are adopted to determine the Young's modulus.[43,52]

It is evident from Fig. 2 that overall Young's modulus E_{ov} determined from EBT-Classical appears a decreasing trend as the cross-sectional size h increases. Basically, it is expected that the surface effect reduces as the cross-sectional size increases, and when h is sufficiently large, E_{ov} would equal to E_b. This expectation is confirmed by the results in Fig. 2. Furthermore, the obvious decreasing pattern

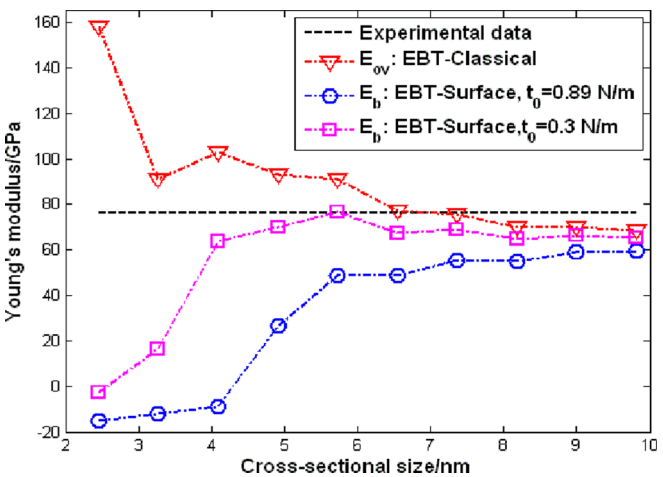

FIG. 2. Comparison of Young's modulus between experimental measurements and theoretical calculations from MD simulation results in Group 1 by EBT-Classical and EBT-Surface. A smaller residual surface stress tensor as 0.3 N/m is considered as well.

of E_{ov} suggests that surface effect has strengthened the NW. The decreasing trend of E_{ov} becomes much steadier with the increasing h, indicating the surface effect reduces. In the meanwhile, Fig. 2 suggests that E_{ov} would eventually fluctuate around a certain value.

On the contrary, bulk Young's modulus E_b obtained from EBT-Surface exhibits an initial increase trend. Specifically, E_b increases with the increase of h, which converges to a certain value (around 65 GPa) when h is fairly large. For relatively small h ($h<4$ nm), Eq. (3b) even predicts a negative value of E_b as illustrated in Fig. 2, which is unreasonable from the viewpoint of continuum mechanics, as E_b is the materials intrinsic property and should be size-independent or insensitive to size. These observations imply that EBT-Surface does not accurately describe the surface effect when the NW possesses a small cross-sectional size. For comparison, another fitting of Eq. (3b) by considering a smaller residual surface stress as $\tau_0 = 0.3\,\mathrm{N/m}$ is also conducted. As shown in Fig. 2, the values of E_b are found uniformly larger than previous one ($\tau_0 = 0.89\,\mathrm{N/m}$), with the converged value almost the same. This finding suggests that the EBT-Surface has overestimated the surface stress effect, especially for the NW with small cross-sectional size.

B. Thick nanowires

Researchers have also considered thick NWs under bending deformation. According to the classical Timoshenko beam theory, the governing equation is given as (referred as TBT-Classical),

$$\begin{cases} (EI)^*\psi'' - a_sAG\psi + a_sAGw' = 0 \\ a_sAGw'' - a_sAG\psi' = 0 \end{cases} \tag{4}$$

where ψ is the angular displacement, and $\psi' = d\psi/dx$, $\psi'' = d^2\psi/dx^2$. G is the bulk shear modulus and a_s is the shear coefficient depending on the cross-sectional shape. The shear coefficient is given as $a_s = 5(1+d)(6+5d)^{-1}$ for a square cross-section beam.[30,57] For double clamped beam subjected to a force F at the midpoint $x = L/2$. The slope at the midpoint is zero because of symmetry, i.e., $\psi(L/2) = 0$. The slope and transverse displacement at $x = 0$ is also zero. The force equilibrium at $x = 0$ is $a_sAG(w' - \psi) = F/2$. Solving Eq. (4) using these boundary conditions, the following relationships between the load F and the maximum displacement d is obtained:

$$F = \left[-\frac{L^3}{96(EI)^*} + \frac{L^3}{64(EI)^*} + \frac{L}{4a_sAG} \right]^{-1} d. \tag{5}$$

Recently, surface effect has also being incorporated into TBT-Classical for thick NWs by several researchers.[30,36,45] The governing equation of the classical Timoshenko beam theory augmented with surface effect is given by (shorted as TBT-Surface)

$$\begin{cases} (EI)^*\psi'' - a_sAG\psi + a_sAGw' = 0 \\ a_sAGw'' - a_sAG\psi' = -Hw'' \end{cases}. \tag{6}$$

The parameter H is replaced by H^0 in considering small deformation approximation. The boundary conditions are similar as TBT-Classical, except the force equilibrium at $x = 0$, which turns out to be $a_sAG(w' - \psi) = F/2 + \int_0^{L/2} Hw''dx$. Hence, the modified relationships between the load F and the maximum displacement d is obtained

$$F = \frac{4\lambda H^0}{L}\left[1 + \frac{4}{\sqrt{k_{ts}}}(k_{ts}\Theta - 1)\tanh\left(\frac{\sqrt{k_{ts}}}{4}\right) \right]^{-1} d, \tag{7}$$

where $\lambda = a_sAG/(a_sAG + H)$, $\Theta = (EI)^*/(a_sAGL^2)$, and $k_{ts} = \lambda H^0 L^2/(EI)^*$. k_{ts} is refereed as the nondimensional surface effect factor under Timoshenko beam theory. Equations (5) and (7) are then compared with MD simulation results of thick Ag NWs in Group 2 with the same length as 24.54 nm and different cross-sectional sizes ranging from 2.454 nm to 9.816 nm (see Table I). The bulk shear modulus G of 30 GPa is adopted.[58]

Figure 3 shows the comparison of estimated Young's modulus by Eqs. (5) and (7). The results obtained from EBT-Classical are also presented. It is found that E_{ov} determined by EBT-Classical decreases continuously with the increase of h. Such unreasonable changing trend has demonstrated the influence of shear deformations in thick NWs and thus indicates the EBT-Classical is no longer applicable for NWs in Group 2. For TBT-Classical, E_{ov} decreases at the beginning, and then appears steady when h passes a threshold value, after that it decreases sharply. Since the length of the NW is constant, thus the increase of h has gradually turned the NW into block materials. When h is too large, e.g., such as 9.816 nm, which makes the slenderness ratio as low as 2.5. Upon such a small slenderness ratio, the bending is more close to an indentation process, leaving the deformation beyond the description by the beam theory. Therefore, only the first two changing periods (p1 and p2) in Fig. 3 have represented the effective prediction by TBT-Classical. Interestingly, these two periods suggest a consistent changing trend of E_{ov} that extracted from EBT-Classical for thin NWs in Fig. 2, i.e., E_{ov} decreases with

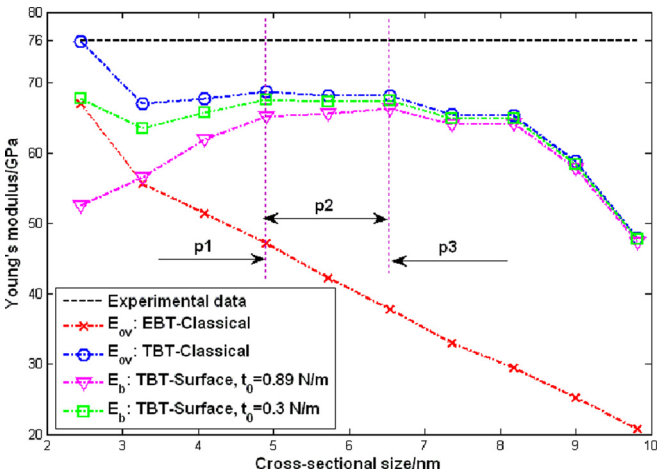

FIG. 3. Comparison of Young's modulus between experimental measurements and theoretical calculations from MD simulation results in Group 2 by EBT-Classical, TBT-Classical, and TBT-Surface. A smaller residual surface stress tensor as 0.3 N/m is considered as well. The whole changing trends of the curves are divided into three parts as p1, p2, and p3. Specifically, p1 refers to the initial changing trend when h is relatively small, p2 refers to the steady changing trend, and p3 refers to the changing trend when h is relatively large.

the increase of cross-sectional size, and converges to a value about 65 GPa when h is fairly large. Therefore, these observations lead to a consistent conclusion that surface effect has strengthened the NW, and the influence is reduced as the NW cross-sectional size increases.

Similar as the result from EBT-Surface for thin NWs (Fig. 2), TBT-Surface also reveals an initial increase and then a steady changing pattern of the overall Young's modulus as depicted in Fig. 3. Thus, we could conclude that the consideration of surface effect in TBT-Surface is also inappropriate when a small cross-sectional size is considered. Another fitting of Eq. (7) with the residual surface stress as $\tau_0 = 0.3\,\mathrm{N/m}$ is presented in Fig. 3 as well. The comparison between τ_0 of 0.89 N/m and 0.3 N/m suggests the same conclusion that the TBT-Surface has overestimated the surface stress effect, especially for a relatively small cross-sectional size.

C. Comparison and discussion

It is obvious from the above discussions that current consideration of the surface effect is suffering some inaccuracy for both thin and thick NWs considered in this work, especially when the NW cross-sectional size is within a relatively small value. Therefore, reconsideration of the surface effect is needed. In this section, we will investigate the possible factors that might lead to the inaccuracy when considering the surface effect. Discussion emphasis is put on thin NWs.

1. Approximation of the axial extension

As aforementioned, all above methods have ignored the axial extension effect during bending deformation. It is acceptable to disregard the axial extension in continuum mechanics, as it has no noticeable effect on the behavior of the beam.[59] However, when the beam size is down to nanoscale, the axial extension is expected to exert obvious influence to the beam behaviors. Through the incremental deformation theory, Song *et al.*[60] developed a new formulation for the Euler-Bernoulli beam, which incorporated effects of the surface stress, surface-induced initial stress and surface elasticity. Basing on the resonant frequency, they found that the surface-induced initial stresses can significantly influence the overall mechanical properties of NWs. Results from both experimental measurements and other MD simulations suggest that when the displacement is larger than one cross-sectional size, the corresponding load-displacement curve during bending will turn out to be nonlinear.[43,52] However, it is apparent that Eqs. (3a) and (3b) only provide a linear solution. In view of this point, we adopt the modified Euler-Bernoulli beam theory augmented with axial extension effect proposed by Heidelberg *et al.*,[52] the governing equation is given as (referred as EBT-Axial)

$$(EI)^* w^{iv} - Tw'' = 0, \tag{8}$$

where T is the axial extension due to bending deformation, it is given by[53]

$$T = (EA)^* \varepsilon_x = \frac{(EA)*}{L} \int_0^{L/2} \left(\frac{dw}{dx}\right)^2 dx. \tag{9}$$

The effective flexural rigidity is utilized in Eq. (8) to account for the surface elasticity. $(EA)^*$ is the effective extensional rigidity,[61] which is written as $(EA)* = EA + 4E_s h$. Solving Eq. (8) with the same boundary conditions applied in Eq. (1), with the force equilibrium at $x = 0$ as $-(EI)w''' = -Tw' + F/2$. The following solution is obtained

$$F = \frac{192(EI)^*}{L^3} f(k_a) d,\ f(k_a) = \frac{k_a}{48 - 192\tanh(\sqrt{k_a}/4)/\sqrt{k_a}}, \tag{10}$$

where k_a is directly connected to the axial tension as $k_a = TL^2/(EI)^*$. Similarly, we refer k_a as axial extension effect factor. According to Eq. (9), the axial extension effect factor is related to the maximum displacement d by the following transcendental equation:

$$\frac{k_a \cosh^2(\sqrt{k_a}/4)}{2 + \cosh(\sqrt{k_a}/2) - 6\sinh(\sqrt{k_a}/2)/\sqrt{k_a}} \times \left(1 - 4\frac{\tanh(\sqrt{k_a}/4)}{\sqrt{k_a}}\right)^2 = d^2 \frac{(EA)^*}{(EI)^*}. \tag{11}$$

Obviously, the above equation is complex in nature and a numerical solution is required. Following asymptotic solution is constructed:

$$k_a = \frac{6s(140 + s)}{350 + 3s}, \quad s = d^2 \frac{(EA)^*}{(EI)^*}. \tag{12}$$

The calculated E_b by Eq. (10) from MD simulation results in Group 1 is presented in Fig. 4(a). As we note that $f(k_a) \geq 1$, means the inclusion of the axial extension increase the effective rigidity of the beam. Thus, E_{ov} determined from the same F-d curve by Eq. (3a) should be essentially larger than E_b by Eq. (10). This trend is approved in Fig. 4(a). In general, E_b determined by EBT-Axial exhibits a general decrease trend with the increase of h, and converges to a certain value when h is fairly large. This changing trend is very close to the E_{ov} determined by EBT-Classical. As shown in Fig. 4(a), E_b obtained from EBT-Axial is around 140 GPa for h equals 2.454 nm, while for the largest h (9.816 nm), E_b is only about 60 GPa. Such big deviation suggests that EBT-Axial also encounters certain inaccuracy in the determination of Young's modulus when h is relatively small.

Figures 4(b) and 4(c) present the fitting and prediction results of F-d curve by Eq. (10). It is clearly seen from Fig. 4(b) that for the smallest h (2.454 nm) considered in this work, the prediction by Eq. (10) shows poor accuracy. On the contrary, for a larger h (6.544 nm) the predictions are much closer to the MD simulation results. These observations indicate that the simple consideration of axial extension is not appropriate for NWs with a relatively small cross-sectional size. In all, as shown in Fig. 4(c), the real importance of EBT-Axial is that it provides a nonlinear solution that accounts for the axial extension induced nonlinear F-d curve, and agrees well with both experimental measurements and MD simulation results.[43,52] According to Fig. 4(b), it is sure that we could improve the EBT-Axial prediction quality

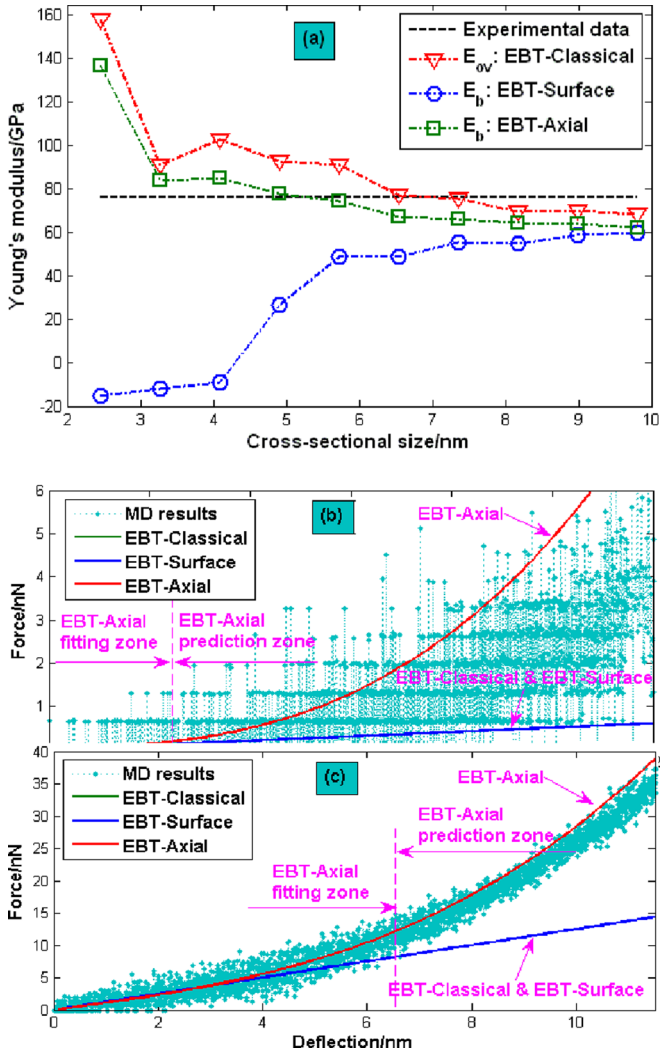

FIG. 4. (a) Comparison of Young's modulus between experimental measurements and theoretical calculations from MD simulation results in Group 1 by EBT-Classical, EBT-Surface, and EBT-Axial; (b) *F-d* curve comparison between the fitting and prediction results from Eq. (10) and MD simulation results when the NW cross-sectional size equals 2.454 nm; (c) *F-d* curve comparison between the fitting and prediction results from Eq. (10) and MD simulation results when the NW cross-sectional size equals 6.544 nm.

by enlarging the fitting zone. Through such procedure, bulk Young's modulus E_b could also be reduced greatly to the value around 70 GPa. Although such results yield good agreement with our expectation (bulk Young's modulus is size-independent or insensitive to size), which actually indicates the shortage of EBT-Axial when NW cross-sectional size is relatively small.

2. Approximation of surface effect

Discussions in previous section have suggested that, the residual surface stress exerts noticeable effect to NW mechanical properties. According to Wang and Feng,[33] the parameter H (see Eq. (2)) for square cross-sectional beam is given as $H = 2\tau h$, and τ is the surface stress given by $\tau = \tau_0 + E_s\varepsilon_x$. Suppose that the axial strain ϵ_x could not be ignored during bending, then $H = H^0 + 2hE_s\varepsilon_x$. Hence, another modified Euler-Bernoulli beam theory could be developed which includes both contributions from the axial effect and surface effect. The governing equation reads (referred as EBT-AS)

$$(EI)^* w^{iv} - (H+T)w'' = 0. \tag{13}$$

Solving Eq. (13), the following solution is obtained:

$$F = \frac{192(EI)^*}{L^3} f(k_{as})d,$$
$$f(k_{as}) = \frac{k_{as}}{48 - 192\tanh(\sqrt{k_{as}}/4)/\sqrt{k_{as}}}, \tag{14}$$

where k_{as} is referred as the axial-surface effect factor, and directly connected to the axial extension and the surface effect as $k_{as} = (H+T)L^2/(EI)^*$. According to Eq. (14), the axial-surface effect factor is related to the maximum displacement d by the following transcendental equation:

$$\left(k_{as} - \frac{H^0L^2}{(EI)^*}\right)\frac{\cosh^2(\sqrt{k_{as}}/4)}{2+\cosh(\sqrt{k_{as}}/2) - 6\sinh(\sqrt{k_{as}}/2)/\sqrt{k_{as}}}$$
$$\times\left(1 - 4\frac{\tanh(\sqrt{k_{as}}/4)}{\sqrt{k_{as}}}\right)^2 = d^2\frac{(EA)^* + 2E_sh}{(EI)^*}. \tag{15}$$

Furthermore, Eq. (15) can be simplified through Taylor expansion as

$$(\text{kas - }\beta)f(k_{as}) = s_1,$$
$$f(k_{as})_{(n=2m+5,m\in N)} = \frac{\frac{1}{12} + \frac{k_{as}}{960} + \ldots + \frac{3n(n-3)}{2^{n-6}(n+1)!}k_{as}^{\frac{n-5}{2}}}{\frac{1}{5} + \frac{k_{as}}{420} + \ldots + \frac{3(n-3)}{2^{n-7}n!}k_{as}^{\frac{n-5}{2}}}, \tag{16}$$

where $\beta = H^0L^2/(EI)^*$, $s_1 = d^2[(EA)^* + 2E_sh]/(EI)^*$. Evidently, Eq. (16) is a transcendental equation of k_{as} regarding parameters β and s_1. In the meanwhile, $f(k_{as})$ is a monotonic increasing function for $k_{as} > 0$, and $5/12 < f(k_{as}) < 1/2$. As is seen, it is still very difficult to obtain an asymptotic solution for Eq. (16). Therefore, to construct a general asymptotic solution we follow the same method employed by Heidelberg *et al.*[52] It is easy to find $k_{as} = 2s_1 + \beta$ from Eq. (16) by assuming s_1 tends to positive infinite. Therefore, the approximate solution is given by superimposing the small and large deflection limits as

$$F = \frac{192(EI)^*}{L^3}d\left(1 + \frac{H^0L^2}{48(EI)^*} + \frac{(EA)^* + 2E_sh}{24(EI)^*}d^2\right). \tag{17}$$

Equation (17) is then employed to fit with MD simulation results in Group 1. From Fig. 5, values of E_b obtained from EBT-AS are very close with those from EBT-Surface, i.e., E_b increases with the increase of cross-sectional size, and converges to a certain value (around 65 GPa) when h is large enough. Such similarity suggests the same conclusion that EBT-AS is suffering certain inaccuracy in interpreting the surface effect. In particular, we find predictions from EBT-AS are even ill-conditioned for h equals 2.454 nm and 3.272 nm. It is thus concluded that considerations of both axial effect and surface effect are still encountered with some inaccuracy when h is relatively small.

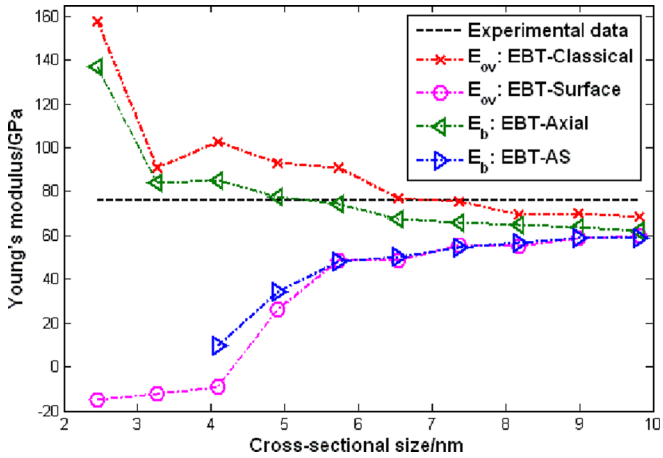

FIG. 5. Comparison of Young's modulus between experimental measurements and theoretical calculations from MD simulation results in Group 1 by EBT-Classical, EBT-Surface, EBT-Axial, and EBT-AS.

3. Ignoring intrinsic stress

Another usual approximation adopted by previous researchers is that there is no residual intrinsic stress existed in NW. Again, such approximation is acceptable in continuum mechanics. However, this is not the case for NW at nanoscale. According to Diao *et al.*,[62] for the $\langle 100\rangle/\{001\}$ NW, the residual intrinsic stress induced by the residual surface stress is estimated to be

$$\sigma = -4\tau h/A = -4\tau/h. \tag{18}$$

The magnitude of σ in NW is on the order of MPa to GPa. Such significant residual intrinsic stress could exert large influence to NW properties. A recent molecular statics study by Liang *et al.* reveals that the nonlinear elasticity of NW core plays a considerably larger role in determining the elastic modulus of NWs subjected to uniaxial loads.[63] Thus, it is of great interest to investigate the intrinsic stress influence on NW bending properties.

As is known, in the absence of external force, the virial stress average over the entire NW is zero after energy minimization or initial relaxation. Following the same procedure by Diao *et al.*,[18] the axial virial stress distribution of the NW along the cross section could be estimated. Particularly, the virial stress in this work is averaged over each column of atoms along the longitudinal direction (around the center region) with the distance of $\Delta x = 4.09$ nm (see Fig. 1(b)). Figure 6 shows the cross-sectional stress distribution of NWs with three different cross-sectional sizes. Just as expected, the residual intrinsic compressive stress increases as the cross-sectional size decreases.[18] Meanwhile, the residual intrinsic stress is observed on the order of GPa. For instance, when $h = 2.46$ nm, the residual surface tensile stress is estimated around 3.5 GPa and the residual intrinsic compressive stress is around 1.5 GPa. Such large compressive stress is supposed to play a crucial role in NW bending behaviors.

However, implementing the residual intrinsic compressive stress effect into the beam theory still encounters with huge complexity, and there is rare explicit discussion suggesting the appropriate estimation of such residual intrinsic stress influence. According to Wang and Feng,[33] the complete surface stress effect is expressed as $H = 2h(\tau_0 + E_s\varepsilon_x)$. Based on the relationship between the surface stress and the intrinsic stress in Eq. (18), we assume the combination effect of the surface stress and the intrinsic stress can be written by μH. Comparing with the surface effect parameter H, this assumption indicates an opposite influence induced by the intrinsic stress as $(\mu - 1)H$. Therefore, a new modified Euler-Bernoulli beam model is proposed, which includes a comprehensive consideration of influences from surface stress, intrinsic stress and axial extension effect. The F-d relationship is thus refined as (referred as EBT-ASI)

$$F = \frac{192(EI)^*}{L^3} d\left(1 + \frac{\mu H^0 L^2}{48(EI)^*} + \frac{(EA)^* + 2\mu E_s h}{24(EI)^*} d^2\right). \tag{19}$$

For Ag NWs applied in this work, we find when μ is around 0.25 the prediction of F-d curve by Eq. (19) agrees well with MD simulation results. As illustrated in Fig. 7(b), the prediction accuracy of F-d curve is found improved significantly by EBT-ASI for the cross-sectional size of 2.454 nm. Such good predictions results are also found for the NW with larger cross-sectional size (e.g., when h equals 5.726 nm as shown in Fig. 7(c)). These findings are encouraging, which not only suggest the influence of intrinsic stress and also the

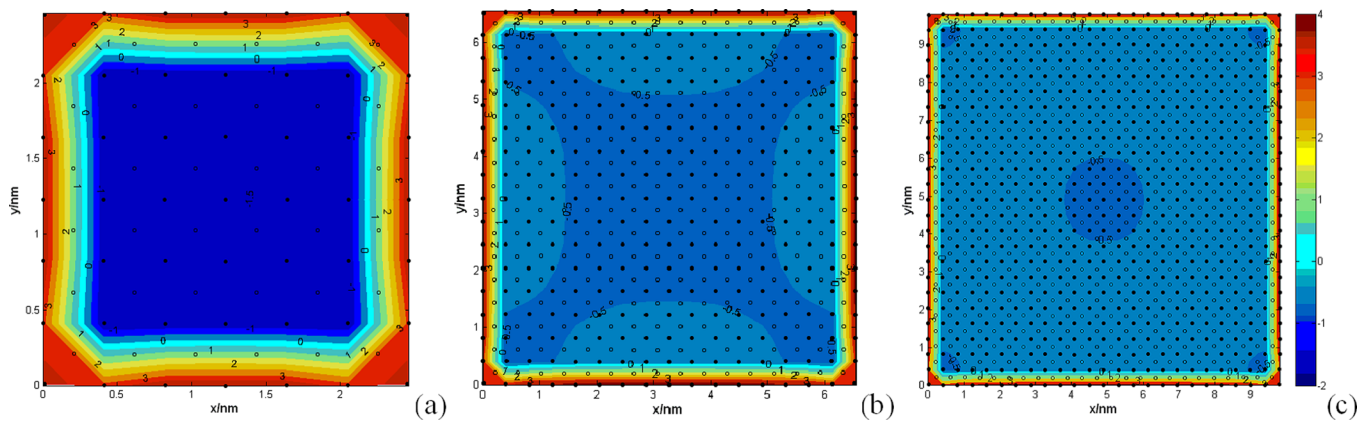

FIG. 6. Axial virial stress distribution along the NW cross section. All three NWs have the same length as 12.27 nm. The virial stress is averaged over each column of atoms along the longitudinal direction (around the center region) with the distance of $\Delta x = 4.09$ nm. (a) NW cross-sectional size equals 2.46 nm; (b) NW cross-sectional size equals 6.54 nm; (c) NW cross-sectional size equals 9.81 nm.

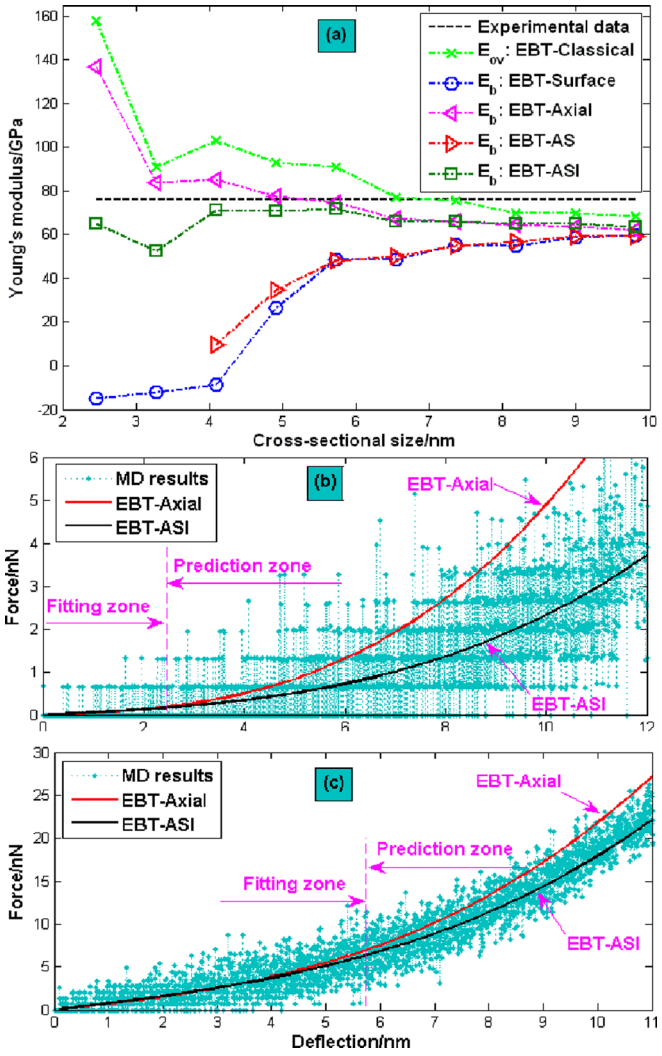

FIG. 7. (a) Comparison of Young's modulus between experimental measurements and theoretical calculations from MD simulation results in Group 1 by EBT-Classical, EBT-Surface, EBT-Axial, EBT-AS, and EBT-ASI; (b) *F-d* curve comparison between the fitting and prediction results from Eqs. (10) and (19), and MD simulation results when the NW cross-sectional size equals 2.454 nm; (c) *F-d* curve comparison between the fitting and prediction results from Eqs. (10) and (19), and MD simulation results when the NW cross-sectional size equals 5.726 nm.

necessity of considering intrinsic stress effect. The estimated E_b of Group 1 from EBT-ASI and other modified theories are compared in Fig. 7(a). The values of E_b are found to fluctuate around 65 GPa, which is satisfied with our expectation, i.e., the bulk Young's modulus is size-independent.

To further examine Eq. (19), we consider another group of simulations, which includes eight NWs with the same slenderness ratio L/h of 15, and the cross-sectional size h varies from 2.454 nm to 8.18 nm (see Table I). As shown in Fig. 8, the estimated E_b from EBT-ASI in this group also appears a fluctuating trend around 65 GPa, which further confirms the intrinsic stress influence. Other two estimations of bulk Young's modulus by EBT-Surface and EBT-AS still show an initial increase and then steady changing trend. These results not only suggest the necessity of the consideration of intrinsic compressive stress but also indicate the overestimation of the surface effect by EBT-Surface and EBT-AS.

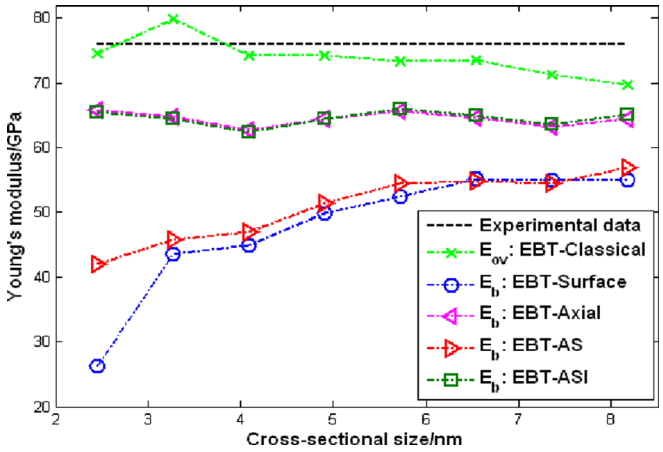

FIG. 8. Comparison of Young's modulus between experimental measurements and theoretical calculations from MD simulation results in Group 3 by EBT-Classical, EBT-Surface, EBT-Axial, EBT-AS, and EBT-ASI.

In the end, it should be noted that, according to Fig. 8, estimations of Young's modulus by EBT-Axial also appear a fluctuating trend around 65 GPa, which almost coincide with the estimations by EBT-ASI. This observation can be explained as follows. Besides of the consideration of axial extension (that caused by later bending) and surface elasticity in EBT-Axial, the residual surface stress and intrinsic stress are also embedded in EBT-ASI. Suppose that the axial extension effect is a superposition of surface stress effect and intrinsic stress effect, and then EBT-ASI could be taken as a more comprehensive consideration of axial extension effect, which accounts for the residual surface stress and intrinsic stress influence. In the meanwhile, for NWs with a relatively large slenderness ratio, the influence of axial extension becomes more predominant than the influence from the residual surface stress and intrinsic stress. Therefore, estimations of Young's modulus by EBT-Axial and EBT-ASI appear very close to each other in Group 3. In all, since the residual intrinsic stress is inherently existed in NWs, therefore, simply considering surface stress effect is inappropriate, especially for NWs with a relatively small cross-sectional size. Moreover, for double clamped NW under large displacement bending, the axial extension exerts larger influence to NW bending behaviors than the residual surface stress.

IV. CONCLUSIONS

Based on the MD simulation, a comprehensive theoretical and numerical study for bending properties of nanowires considering surface/intrinsic stress effects and axial extension effect is carried out. The surface effect is observed to strengthen the NW, and the influence reduces as the NW cross-sectional size increases. The initially discussed theories include the Euler-Bernoulli beam theory and Timoshenko beam theory augmented with surface effect. It is found that when the NW possesses a relatively small cross-sectional size, these two theories cannot accurately interpret the true surface effect. The incorporation of the axial extension effect into the Euler-Bernoulli beam theory has provided a nonlinear solution that agrees with the nonlinear-

elastic experimental and simulation results. However, there is still some inaccuracy when the NW cross-sectional size is relatively small. Modified Euler-Bernoulli beam theory includes both contributions from surface effect and axial extension effect has been developed, which still appears an inappropriate determination of Young's modulus.

Basically, residual intrinsic stress is inherently accompanied by residual surface stress for NWs. A relatively large residual intrinsic stress is observed in NWs, which is supposed to play a crucial role in NW bending behaviors, especially when a relatively small cross-sectional size is considered. A comprehensive model for completely considering influences from surface stress effect, intrinsic stress effect, and axial extension effect is proposed, which shows good agreement with MD simulation results, indicating it is necessary to account for the intrinsic stress influence on NW bending behavior. In all, it is summarized that, for NWs with a relatively large cross-sectional size under small bending displacement (e.g., the displacement is smaller than half cross-section size), both Euler-Bernoulli beam theory and Timoshenko beam theory augmented with surface effect show good agreement with simulation results. Therefore, both theories are applicable. However, for thin NWs, the consideration of axial extension effect is needed when the displacement is relatively large (e.g., displacement larger than one cross-sectional size). For NWs with a relatively small cross-sectional size, the simple consideration of surface stress effect is inappropriate, and a comprehensive consideration of the intrinsic stress effect is required.

[1]M. Kawamura, N. Paul, V. Cherepanov, and B. Voigtländer, Phys. Rev. Lett. **91**, 96102 (2003).
[2]A. Husain, J. Hone, H. W. C. Postma, X. Huang, T. Drake, M. Barbic, A. Scherer, and M. Roukes, Appl. Phys. Lett. **83**, 1240 (2003).
[3]M. Li, T. S. Mayer, J. A. Sioss, C. D. Keating, and R. B. Bhiladvala, Nano Lett. **7**, 3281 (2007).
[4]D. Rugar, R. Budakian, H. Mamin, and B. Chui, Nature **430**, 329 (2004).
[5]Y. Yang, C. Callegari, X. Feng, K. Ekinci, and M. Roukes, Nano Lett. **6**, 583 (2006).
[6]K. Eom, H. S. Park, D. S. Yoon, and T. Kwon, Phys. Rep. **503**, 115 (2011).
[7]N. Hu, Y. Karube, M. Arai, T. Watanabe, C. Yan, Y. Li, Y. Liu, and H. Fukunaga, Carbon **48**, 680 (2010).
[8]T. Palacios, Nature **481**, 152 (2012).
[9]M. Riaz, O. Nur, M. Willander, and P. Klason, Appl. Phys. Lett. **92**, 103118 (2008).
[10]J. Song, X. Wang, E. Riedo, and Z. L. Wang, Nano Lett. **5**, 1954 (2005).
[11]S. Hoffmann, I. Utke, B. Moser, J. Michler, S. H. Christiansen, V. Schmidt, S. Senz, P. Werner, U. Gösele, and C. Ballif, Nano Lett. **6**, 622 (2006).
[12]L. W. Ji, S. J. Young, T. H. Fang, and C. H. Liu, Appl. Phys. Lett. **90**, 033109 (2007).
[13]Y. Yue, P. Liu, Z. Zhang, X. D. Han, and E. Ma, Nano Lett. **11**, 3151 (2011).
[14]J. H. Seo, Y. Yoo, N. Y. Park, S. W. Yoon, H. Lee, S. Han, S. W. Lee, T. Y. Seong, S. C. Lee, and K. B. Lee, Nano Lett. **11**, 3499 (2011).
[15]Y. Zhu, Q. Qin, F. Xu, F. Fan, Y. Ding, T. Zhang, B. J. Wiley, and Z. L. Wang, Phys. Rev. B **85**, 045443 (2012).
[16]H. S. Park and J. A. Zimmerman, Phys. Rev. B **72**, 54106 (2005).
[17]K. Gall, J. Diao, and M. L. Dunn, Nano Lett. **4**, 2431 (2004).
[18]J. Diao, K. Gall, and M. L. Dunn, J. Mech. Phys. Solids **52**, 1935 (2004).
[19]H. F. Zhan, Y. T. Gu, C. Yan, X. Q. Feng, and P. Yarlagadda, Comput. Mater. Sci. **50**, 3425 (2011).
[20]P. A. T. Olsson and H. S. Park, Acta Mater. **59**, 3883 (2011).
[21]S. Jiang, H. Zhang, Y. Zheng, and Z. Chen, J. Phys. D: Appl. Phys. **42**, 135408 (2009).
[22]H. F. Zhan, Y. T. Gu, C. Yan, and P. K. D. V. Yarlagadda, Adv. Mater. Res. **335**, 498 (2011).
[23]Y. Zheng, H. Zhang, Z. Chen, L. Wang, Z. Zhang, and J. Wang, Appl. Phys. Lett. **92**, 041913 (2008).
[24]M. McDowell, A. Leach, and K. Gall, Modell. Simul. Mater. Sci. Eng. **16**, 045003 (2008).
[25]H. Wu, Comput. Mater. Sci. **31**, 287 (2004).
[26]J. Diao, K. Gall, and M. L. Dunn, Nat. Mater. **2**, 656 (2003).
[27]H. S. Park, K. Gall, and J. A. Zimmerman, Phys. Rev. Lett. **95**, 255504 (2005).
[28]W. Liang, M. Zhou, and F. Ke, Nano Lett. **5**, 2039 (2005).
[29]H. S. Park and C. Ji, Acta Mater. **54**, 2645 (2006).
[30]G. F. Wang and X. Q. Feng, J. Phys. D: Appl. Phys. **42**, 155411 (2009).
[31]G. F. Wang and X. Q. Feng, EPL (Europhysics Letters) **91**, 56007 (2010).
[32]G. Wang and X. Feng, Appl. Phys. Lett. **94**, 141913 (2009).
[33]G. F. Wang and X. Q. Feng, Appl. Phys. Lett. **90**, 231904 (2007).
[34]J. He and C. M. Lilley, Nano Lett. **8**, 1798 (2008).
[35]J. He and C. M. Lilley, in *8th IEEE Conference on Nanotechnology* (Arlington, TX 2008), p. 565.
[36]L. Jiang and Z. Yan, Physica E (Amsterdam) **42**, 2274 (2010).
[37]J. Wang, Z. Huang, H. Duan, S. Yu, X. Feng, G. Wang, W. Zhang, and T. Wang, Acta Mechanica Solida Sinica **24**, 52 (2011).
[38]H. Park and P. Klein, Phys. Rev. B **75**, 85408 (2007).
[39]G. Yun and H. Park, Phys. Rev. B **79**, 195421 (2009).
[40]P. A. T. Olsson, H. S. Park, and P. C. Lidström, J. Appl. Phys. **108**, 104312 (2010).
[41]B. Wu, A. Heidelberg, and J. J. Boland, Nat. Mater. **4**, 525 (2005).
[42]B. Wu, A. Heidelberg, J. J. Boland, J. E. Sader, X. M. Sun, and Y. D. Li, Nano Lett. **6**, 468 (2006).
[43]H. F. Zhan and Y. T. Gu, Comput. Mater. Sci. **55**, 73 (2012).
[44]S. Plimpton, J. Comput. Phys. **117**, 1 (1995).
[45]C. Liu and R. Rajapakse, IEEE Trans. Nanotechnol. **9**, 422 (2010).
[46]A. Voter, Los Alamos Unclassified Technical Report LA-UR, 93 (1993).
[47]R. Smith, C. Nock, S. Kenny, J. J. Belbruno, M. Di Vece, S. Palomba, and R. Palmer, Phys. Rev. B **73**, 125429 (2006).
[48]S. Plimpton, J. Comput. Phys. **117**, 1 (1995).
[49]W. G. Hoover, Phys. Rev. A **31**, 1695 (1985).
[50]S. Nosé, J. Chem. Phys. **81**, 511 (1984).
[51]G. Jing, H. Duan, X. Sun, Z. Zhang, J. Xu, Y. Li, J. Wang, and D. Yu, Phys. Rev. B **73**, 235409 (2006).
[52]A. Heidelberg, L. T. Ngo, B. Wu, M. A. Phillips, S. Sharma, T. I. Kamins, J. E. Sader, and J. J. Boland, Nano Lett. **6**, 1101 (2006).
[53]L. Landau and E. Lifshitz, *Theory of Elasticity* (Butterworth-Heinemann, Oxford, 1986).
[54]J. Gere and S. Timoshenko, *Mechanics of Materials*, 4th ed. (Cheltenham, Stanley Thornes, 1999).
[55]T. Chen, M. S. Chiu, and C. N. Weng, J. Appl. Phys. **100**, 074308 (2006).
[56]V. Shenoy, Phys. Rev. B **71**, 94104 (2005).
[57]J. R. Hutchinson, J. Appl. Mech. **68**, 87 (2001).
[58]Y. Akahama, H. Kawamura, and A. K. Singh, J. Appl. Phys. **95**, 4767 (2004).
[59]S. P. Timoshenko and J. M. Gere, *Theory of Elastic Stability* (McGraw-Hill, New York, 1961).
[60]F. Song, G. Huang, H. Park, and X. Liu, Int. J. Solids Struct. **48**, 2154 (2011).
[61]R. Miller and V. Shenoy, Nanotechnology **11**, 139 (2000).
[62]J. Diao, K. Gall, M. Dunn, and J. Zimmerman, Acta Mater. **54**, 643 (2006).
[63]H. Liang, M. Upmanyu, and H. Huang, Phys. Rev. B **71**, 241403 (2005).